www.nature.com/aps

Acta Pharmacologica Sinica

ARTICLE

Characterization of LTr1 derived from cruciferous vegetables as a novel anti-glioma agent via inhibiting TrkA/PI3K/AKT pathway

Qi-qi Song[1], Li-ping Lin[2], Ya-li Chen[1], Jia-cheng Qian[2], Ke Wei[1], Jian-wei Su[1], Jian-hua Ding[3], Ming Lu[3], Yang Liu[1], Ren-xiang Tan[2,4] and Gang Hu[1,3]

Malignant glioma is the most fatal, invasive brain cancer with limited treatment options. Our previous studies show that 2-(indol-3-ylmethyl)-3,3′-diindolylmethane (LTr1), a major metabolite of indole-3-carbinol (I3C) derived from cruciferous vegetables, produces anti-tumour effect against various tumour cell lines. In this study we characterized LTr1 as a novel anti-glioma agent. Based on screening 134 natural compounds and comparing the candidates' efficacy and toxicity, LTr1 was selected as the lead compound. We showed that LTr1 potently inhibited the viability of human glioma cell lines (SHG-44, U87, and U251) with IC_{50} values of 1.97, 1.84, and 2.03 μM, respectively. Furthermore, administration of LTr1 (100,300 mg·kg^{-1}·d^{-1}, i.g. for 18 days) dose-dependently suppressed the tumour growth in a U87 xenograft nude mouse model. We demonstrated that LTr1 directly bound with TrkA to inhibit its kinase activity and the downstream PI3K/AKT pathway thus inducing significant S-phase cell cycle arrest and apoptosis in SHG-44 and U87 cells by activating the mitochondrial pathway and inducing the production of reactive oxygen species (ROS). Importantly, LTr1 could cross the blood-brain barrier to achieve the therapeutic concentration in the brain. Taken together, LTr1 is a safe and promising therapeutic agent against glioma through inhibiting TrkA/PI3K/AKT pathway.

Keywords: malignant glioma; 2-(indol-3-ylmethyl)-3,3′-diindolylmethane (LTr1); TrkA; reactive oxygen species; S phase cell cycle arrest; mitochondrial pathway; paclitaxel; cruciferous vegetables

Acta Pharmacologica Sinica (2023) 44:1262–1276; https://doi.org/10.1038/s41401-022-01033-y

INTRODUCTION

Cruciferous plants, including broccoli, cabbage, mustard, Chinese cabbage, and cauliflower, are some of the most popular and extensively cultivated vegetables in the world due to their nutritious properties and notable health benefits [1]. The consumption of cruciferous vegetables has been associated with a low risk of developing different cancers [2]. Malignant glioma is the most lethal, invasive, and neurologically destructive brain cancer, and these properties lead to poor treatment effects, inferior recovery, and short median survival rates that are observed in patients with glioma [3]. Glioma has a 5-year overall survival rate lower than 5%, and it is challenging to cure glioma because there are limited treatment options [4, 5]. The standard treatment for newly diagnosed gliomas after surgery is the first-line alkylating chemotherapeutic drug TMZ in combination with radiotherapy. However, most patients eventually exhibit resistance to TMZ, which leads to treatment failure. Therefore, there is an urgent need to develop new and more specific therapeutic approaches for the treatment of glioma.

2-(Indol-3-ylmethyl)-3,3′-diindolylmethane (LTr1) is a trimer that is derived from indole-3-carbinol (I3C), which is a well-known anticancer molecule that is widely distributed in cruciferous vegetables. Previously, our group discovered that LTr1 could kill acute myelocytic leukemia (AML) cells that harbour FMS-like tyrosine kinase 3 (FLT3) receptor mutations by inhibiting the FLT3 phosphorylation and the expression of downstream proteins [6]. Furthermore, we found that LTr1 had antitumour activities in various tumour cell lines as well, such as breast cancer (MCF-7), lung cancer (A549), and liver cancer (HepG2) cell lines [7]. Accordingly, LTr1 is considered to be a potent tumour inhibitor superior to that of I3C and 3,3′-diindolylmethane (DIM), of these, DIM is the most active and effective metabolite and it is in phase II/III trials to determine its efficacy in patients with breast cancer or prostate cancer [8, 9]. However, the effect of LTr1 on glioma remains unknown.

It is generally believed that natural products, especially those derived from food, are less toxic than chemically synthesized compounds. Furthermore, the diversity and complexity of natural compounds in chemical structure and their significant advantage in biological activities endow them with privilege as lead compounds. Many studies have suggested that substantial number of naturally derived products exert good effects on glioma-cell proliferation,

[1]Departments of Pharmacology, School of Medicine and Holistic Integrative Medicine, Nanjing University of Chinese Medicine, Nanjing 210023, China; [2]State Key Laboratory Cultivation Base for TCM Quality and Efficacy, Nanjing University of Chinese Medicine, Nanjing 210023, China; [3]Jiangsu Key Laboratory of Neurodegeneration, Department of Pharmacology, Nanjing Medical University, Nanjing 211100, China and [4]State Key Laboratory of Pharmaceutical Biotechnology, Institute of Functional Biomolecules, Nanjing University, Nanjing 210023, China
Correspondence: Yang Liu (liuyang@njucm.edu.cn) or Ren-xiang Tan (rxtan@nju.edu.cn) or Gang Hu (ghu@njmu.edu.cn)
These authors contributed equally: Qi-qi Song, Li-ping Lin

Received: 16 May 2022 Accepted: 15 November 2022
Published online: 8 December 2022

apoptosis, and sensitivity to chemotherapeutic drugs [10–12]. Accordingly, 134 natural compounds that were isolated from cruciferous vegetables or actinomycetes in our laboratory were screened in order to develop novel anti-glioma treatments.

Interestingly, LTr1 and seven other compounds were identified from the 134 natural compounds and exhibited potential anti-glioma activity. However, the other compounds showed the equivalent IC_{50} values against human glioma and normal glial cells, indicating that they did not have safe concentrations at which they could be used as lead compounds. In the present study, we further showed that LTr1 inhibited the proliferation of glioma cells by inducing S-phase cell cycle arrest and apoptosis via mitochondrial pathway activation and reactive oxygen species (ROS) production. Furthermore, LTr1 inhibited TrkA kinase activity and decreased its expression, which in turn inhibited the downstream PI3K/AKT pathway. Moreover, LTr1 inhibited tumour growth and induced apoptosis in the U87 xenograft nude mice model. Promisingly, LTr1 could cross the blood-brain barrier without causing apparent toxicity, suggesting that LTr1 is a potent drug candidate for the treatment of glioma cancer.

MATERIALS AND METHODS

Chemicals and materials

One hundred thirty-four compounds were extracted from cruciferous vegetables or actinomycetes. Paclitaxel (PTX) (S1150) and temozolomide (TMZ) (S1237) were purchased from Selleck Chemicals (Houston, TX, USA). In the experiments in vitro, all compounds were dissolved in DMSO (D2650, Sigma-Aldrich, St. Louis, MO, USA). Paclitaxel injection was purchased from Haikou Pharmaceutical Factory Co (H10980170, Haikou, China). LTr1 was dissolved in DMSO and diluted with corn oil (C116025, Aladdin Chemical Co, Shanghai, China).

The synthesis of LTr1

LTr1 was synthesized according to the reference [13].

Cell lines and cell cultures

Human glioma cell lines SHG-44, U87, U251, and human normal glial cell line (SVG p12) were purchased from the Cell Bank of the Chinese Academy of Sciences (Shanghai, China). All cell lines were cultured in DMEM (12100046, Thermo Fisher Scientific, Waltham, MA, USA) supplemented with 10% FBS (10099141C, GIBCO BRL, Grand Island, NY, USA), 100 U/mL penicillin, and 100 μg/mL streptomycin (C100C5, New Cell & Molecular Biotech Co, Suzhou, China). Mouse primary astrocyte was isolated from brain tissue of neonatal C57BL/6 J mice aged 1–3 days. C57BL/6J mice were purchased from the Experimental Animal Center of Nanjing Medical University (Nanjing, China). The meninges and basal ganglia were removed under a microscope and digested with 0.25% trypsin (G4001, Servicebio, Wuhan, China), and the reaction was terminated with FBS. The suspension was filtered with a 40 μm filter (BD Falcon, San Jose, CA, USA) and centrifuged at $1000 \times g$ for 5 min. The cells were resuspended in DMEM complete medium and then seeded in the 96-well plant or 6-well plate. Cells were incubated at 37 °C in a 5% CO_2 atmosphere.

Animals

All animal care and procedures were performed following national and international guidelines and were approved by the Animal Resource Centre, Nanjing Medical University. We complied with all relevant ethical regulations for animal testing and research. Four-to-five-week-old female nude mice were purchased from Vital River (Beijing Vital River Laboratory Animal Technology Co., Ltd, Beijing, China) and housed in a specific-pathogen-free (SPF) facility under a constant photoperiod (12 h light and 12 h dark) and free access to chaw and sterilized water.

Subcutaneously heterotopic xenograft glioma model

U87 cells (3×10^6/100 μL) were injected subcutaneously into the right flank of mice. When the tumour solids grew to a volume of approximate 50 mm^3, mice were randomized into five groups ($n = 6$) and designated as control, vehicle control [corn oil, intragastric administration (i.g.)], low-dose group (LTr1, 100 mg·kg^{-1}·d^{-1}, i.g.), high-dose group (LTr1, 300 mg·kg^{-1}·d^{-1}, i.g.), and positive control group [paclitaxel, 20 mg/kg, intravenous administration (i.v.)], respectively. The tumour volume (length × width × width/2) and body weight of the mice were monitored every two days. At the end of treatment, mice were sacrificed. The tissues were excised, weighed, processed for histology, and evaluated by hematoxylin and eosin (H&E) staining, immunohistochemical examination, or immunoblotting according to the manufacturer's instructions.

Orthotopic xenograft glioma model

After anesthetizing the nude mice, U87 cells (1×10^6) were injected into the 2 mm lateral midline of the skull. The depth is 3.5 mm. On the third day, mice were randomized into four groups ($n = 6$–8) and designated as vehicle control (corn oil, i.g.), low-dose group (LTr1, 100 mg·kg^{-1}·d^{-1}, i.g.), high-dose group (LTr1, 300 mg·kg^{-1}·d^{-1}, i.g.), and positive control group (paclitaxel, 20 mg/kg, i.v.), respectively. At the end of treatment, mice were narcotized by isoflurane (R510-22-10, RWD Life Science, Shenzhen, China) and then conducted nuclear magnetic resonance (NMR) imaging (Biospec 7T/20 USR, Bruker, Germany). The contrast medium is gadopentetate dimeglumine. Anatomical structures were visualized by T1-weighted imaging consisting of a 3D-spoiled turbo spin echo sequence (256 × 256 matrix, 2 × 22 mm FOV, TR = 300 ms, TE = 8.9 ms, ST = 0.8 mm). Mice were sacrificed, and livers and lungs were excised and processed for histology evaluated by H&E staining.

Analysis of LTr1 by LC-MS/MS

Plasma and tissues from animals: Mice were gavaged with LTr1 at 300 mg/kg dosage and executed to collect blood, brain, heart, liver, spleen, lung, kidney, muscle, and intestines after 3, 6, and 24 h. Blood was centrifuged at 8000 r/min for 10 min to obtain plasma. Tissues taken from tested mice were chopped, accurately weighed, and ground into homogenates with liquid nitrogen in deionized water, respectively.

Sample preparation: Plasma and homogenate samples (50 or 100 μL) were extracted by 2.5-fold volumes of ethyl acetate containing ketoconazole 50 ng/L for concentration determination of LTr1 in plasma and tissues from mice as internal standard (Supplementary Fig. S3). The mixture was vortex-mixed for 3 min and then centrifuged at 8000 r/min for 10 min. The supernatant (200 or 450 μL) was transferred and evaporated to dryness under a vacuum at 30 °C. The residues were resuspended in 200 μL of methanol and centrifugated at 13,000 r/min for 10 min twice. A 2 μL aliquot of the supernatant from each sample was injected for the LC-MS/MS analysis.

Calibration curve and quantification: Working solutions of LTr1 with concentrations in the range of 1–200 μg/mL were obtained by serially diluting the stock solution with methanol. All solutions were stored at 4 °C and brought to room temperature before use. The calibration standards were prepared by spiking the series of working solutions (2.5 or 5 μL) into blank plasma or tissues (47.5 or 95 μL) to yield LTr1 concentrations of 0.005, 0.05, 0.1, 0.25, 0.5, 1, 2.5, 5, 10 and 20 μg/mL.

Chromatography condition: The chromatographic separation was carried out using a Waters BEH C18, 2.1 mm × 100 mm, 1.7 μm column (Waters, USA), on a VANQUISH Thermo UHPLC system (Thermo Fisher Scientific, Waltham, MA, USA). The column oven temperature was set at 40 °C. A mobile phase consisting of 0.025% formic acid in water (A) and acetonitrile (B) was delivered at a flow rate of 0.3 mL/min using the following gradient program: 10% (B)

from 0–1 min, 10%–100% (B) from 1–5 min, 100% (B) from 5–8 min, 100%–10% (B) from 8–10 min for concentration determination of LTr1 in plasma and tissues from animals.

Mass spectrometry conditions: Quantitation was performed by TSQ Quantis triple quadrupole mass spectrometer (Thermo Fisher Scientific, Waltham, MA, USA). The mass operation parameters were set as follows: a negative turbine spray ion source. LTr1 was monitored via selective reaction monitoring (SRM). The precursor-to-product ion pairs for SRM transitions were at *m/z* 374 → 116.071 for LTr1.

Transfection

SHG-44 and U87 cells were cultured and inoculated in the culture plate. TrkA siRNA was transfected by Lipofectamine®3000 (L3000015, Invitrogen, CA, USA) according to the instructions. The fresh culture medium was replaced 6–8 h after transfection, and these dishes were cultured for an additional 48 h. The siRNA sequence is as follows:

NC sense: 5′-UUCUCCGAACGUGUCACGUTT-3′,
antisense: 5′-ACGUGACACGUUCGGAGAATT-3′;
TrkA-1 sense: 5′-CCAUGUCCCUGCAUUUCAUTT-3′,
antisense: 5′-AUGAAAUGCAGGGACAUGGTT-3′;
TrkA-2 sense: 5′-CCUUUCUACGCUGCUCCUUTT-3′,
antisense: 5′-AAGGAGCAGCGUAGAAAGGTT-3′.

Cell viability assay and lactate dehydrogenase (LDH) release assay

Exponentially growing cells were seeded into 96-well plates (4×10^3 cells/well) for 24 h. All compounds were diluted with culture medium to specified concentrations. Cells were treated with compounds for the indicated times and concentrations. Cell viability was determined by cell counting kit-8 (CCK-8) assay (B34304, Bimake; Houston, TX, USA). The half-maximal inhibitory concentration (IC_{50}) was calculated according to GraphPad Prism 8.0 software (GraphPad; San Diego, CA, USA). For LDH release, cell culture supernatants were collected after various treatments, and the LDH activity was detected using the LDH assay kit (C0016, Beyotime Biotechnology, Shanghai, China). The absorbance was measured at 450 nm on a spectrophotometric microplate reader (Thermo Fisher Scientific, Waltham, MA, USA).

Hoechst 33342 staining

Hoechst 33342 staining assay was performed according to the manufacturer's instructions (C1025; Beyotime Biotechnology, Shanghai, China). SHG-44 and U87 cells were cultured in 24-well plates and subjected to the indicated treatments. Hoechst 33342 was added and then incubated for 10 min in the dark to visualize under a fluorescence microscope (Olympus, Tokyo, Japan).

Apoptosis and cell cycle evaluation by flow cytometry

For cell apoptosis or cell cycle analysis, SHG-44 and U87 cells were seeded in 6-well plates and separately treated with indicated concentrations of LTr1 and paclitaxel for 48 h. According to the instruction, cells were treated with Annexin V-FITC/PI Apoptosis Detection Kit (A211, Vazyme Biotech Co., Ltd., Nanjing, China) or Cell Cycle Detection Kit (KGA512, KeyGEN BioTECH, Nanjing, China). Then cells were analyzed with a flow cytometer (Guava Easycyte™8, Millipore, USA).

Determination of ROS production

The production of intracellular ROS and mitochondrial ROS was detected using fluorescent dye H2DCF-DA(D399, Invitrogen, Carlsbad, CA, USA) and MitoSOX™ Red (M36005, Invitrogen, Carlsbad, CA, USA) by observing under a fluorescence microscope or analyzing by flow cytometer. SHG-44 and U87 cells were seeded in 12-well plates and then treated with the indicated concentration of LTr1 and paclitaxel for 48 h. Cells were incubated with H2DCF-DA or MitoSOX staining solution at 37 °C for 30 min in the dark. After 4% paraformaldehyde fixation of cells, Hoechst 33342 was added and then observed under a fluorescence microscope or directly analyzed by flow cytometer (Guava Easycyte™8, Millipore, USA).

Immunoblotting

Cells were washed with cold PBS three times and lysed in the radioimmunoprecipitation assay (RIPA) lysis buffer (KGP702, KeyGEN BioTECH, Nanjing, China) containing protease or phosphatase inhibitors. Mitochondria were extracted with Cell Mitochondria Isolation Kit (C3601, Beyotime, Shanghai, China). Then, extracted proteins were quantitated by the BCA method and denatured by boiling at 95 °C for 5 min. Protein samples were separated by sodium dodecyl sulfate-polyacrylamide gel electrophoresis (SDS-PAGE) and transferred to hydrophobic polyvinylidene (PVDF) membranes, which were blocked with 10% skim milk in Tris-buffered saline with Tween solution (TBST; pH 7.4, 10 mM Tris-HCl, 150 mM NaCl, 0.1% Tween-20) for 1 h at room temperature. Then, the membranes were incubated at 4 °C overnight with primary antibodies against caspase-3 (1:1000, 9662s, Cell Signaling Technology, Beverly, CA, USA), Bcl-2 (1:800, BS1511, Bioworld Technology, Louis Park, MN, USA), Bax (1:2000, 50599-2-Ig, Proteintech, Chicago, IL, USA), caspase-9 (1:1000, 66169-1-Ig, Proteintech), cytochrome *c* (cyto *c*; 1:1000, 66264-1-Ig, Proteintech), PI3K (1:1000, 4249s, Cell Signaling Technology), P-PI3K (1:1000, 4228s, Cell Signaling Technology), AKT (1:1000, 21054-2, SAB, Maryland, USA), P-AKT (1:1000, 11054, SAB), CDK4 (1:1000, 32073, SAB), CDK2 (1:1000, 2546, Cell Signaling Technology), cyclin A2 (1:1000, GB111132, Servicebio, Wuhan, China), p21 (1:500, ab7960, Abcam, Cambridge, UK), TrkA (1:1000, BS91373, Bioworld Technology), β-actin (1:3000, GB12001, Servicebio). COX IV (1:1000, 250135, Zen-bioscience, Chengdu, China). After washing with TBST three times, membranes were incubated with the secondary antibodies of HRP-conjugated goat anti-rabbit IgG (H + L) (1:1000; GB23303, Servicebio) or HRP-conjugated goat anti-mouse IgG (H + L) (1:1000; GB23301, Servicebio) for 2 h at room temperature. Bands were detected by Novex™ ECL Chemiluminescent Substrate Reagent Kit (34580, Thermo Fisher Scientific, Waltham, MA, USA) using an ImageQuant LAS 4000 mini (GE Healthcare, Connecticut, USA).

Assays for TrkA inhibition by LTr1, LOXO-101

Enzyme activity assays were performed according to the manufacturer's instructions using TrkA Kinase Assay Kit (V2931, Promega, Madison, WI, USA). The IC_{50} was calculated according to enzyme activity values using GraphPad Prism 8.0 software.

Immunocytochemical staining

SHG-44 and U87 cells were seeded in 12-well plates and treated with indicated concentrations of LTr1 and paclitaxel for 48 h, respectively. Cells were rinsed with PBS and fixed with 4% paraformaldehyde. After being blocked with PBST containing 5% bovine serum albumin (BSA), the cells were further incubated with the primary antibody against γ-H2AX (1:200, 9718, Cell Signaling Technology) at 4 °C overnight. After washing, cells were exposed to the secondary antibody, Alexa Fluor 488 goat anti-mouse IgG (1:1000, R37120, Invitrogen, Carlsbad, CA, USA) for 1 h at room temperature. After washing and treatment with Hoechst 33342, cells were observed under a fluorescence microscope.

Histopathologic examination

The tumours, kidneys, livers, and spleens were excised and fixed in 4% paraformaldehyde, dehydrated by ethanol, and embedded in paraffin. The paraffin-embedded tissue samples were sectioned into 5 μm slices and then stained with H&E. The histological features were observed and captured under a microscope (Olympus, Tokyo, Japan).

TUNEL staining

TUNEL staining was performed according to the manufacturer's instructions by TUNEL BrightGreen Apoptosis Detection Kit (A112,

Vazyme Biotech Co., Ltd., Nanjing, China). The results were observed under a fluorescence microscope (Olympus, Tokyo, Japan).

Immunohistochemistry assay

Tumour tissues were fixed in 4% paraformaldehyde, embedded in paraffin, and sliced for examination. Thus, obtained slices were stained and analyzed by immunohistochemical inspection. Briefly, the slices were maintained at 60 °C for 2 h, deparaffinized, rehydrated, and unmasked by being submerged into boiling sodium citrate buffer (10 mM, pH 6.0) for 10 min before being treated with 3% H_2O_2 for 10 min. The slices were blocked with 5% BSA in PBS for 1 h at room temperature and then hybridized with anti-Ki67 antibody (1:200, ab15580, Abcam, Cambridge, MA, USA) at 4 °C overnight. After being washed with PBS, the slices were hybridized with the secondary antibodies for 1 h at room temperature, and the results were visualized by the DAB reaction. Images were blindly taken at random fields under a microscope (Olympus, Tokyo, Japan).

Molecular docking

The three-dimensional structure of receptor protein TrkA was obtained from the PDB database (https://www.rcsb.org/pdb, PDB ID: 6D20) [14], and the structure of ligand LTr1 was constructed by Discovery Studio Visualizer. Then the ligand was docked to the active site of the receptor TrkA by the AutoDock program to obtain the protein-ligand complex [15]. Only the polar hydrogen atoms were added to the molecules, and all the atoms were assigned the AD4 type and Gasteiger charge. Lamarckian genetic algorithm was used for the docking process, in which the receptor was kept rigid while the ligand was flexible. All other settings adopted the default values of the program.

Microscale Thermophoresis (MST) analysis

Microscale Thermophoresis assay was performed according to the manufacturer's instructions using the Red-tris-NTA His-tag kit (MO-LO18, Nanotemper, Germany). The labeled TrkA (25 nM) in PBS (pH 7.6) containing 0.05% Tween-20 was incubated with LTr1 for 5 min in a dose range of 0.003–50 μM. After TrkA (11073-H07H2, Sino Biological, Beijing, China) protein labeling and sample preparation, K_D was measured by Monolith NT.115 Pico (Nanotemper Technologies, Germany), using the following parameters: MST-Power Medium, Excitation-Power 5%, Excitation type Pico-RED.

Biolayer interferometry

Ni-NTA biosensors were previously loaded with His-tagged TrkA and then incubated with LTr1 to generate an association curve. The 60-s association phase was subsequently followed by a 90-s dissociation step.

Statistical analysis

All data were representative of at least three independent experiments. Quantitative data are expressed as means ± standard error (SEM). Statistical significance was determined using GraphPad Prism 8.0 software, one-way ANOVA or two-way ANOVA was conducted according to test requirements. *P* values less than 0.5 were statistically significant. $^{*}P < 0.05$; $^{**}P < 0.01$; $^{***}P < 0.001$.

RESULTS

LTr1 was identified as a potent anti-glioma agent from among 134 natural compounds

To discover lead compounds with anti-glioma activity, 134 compounds that were derived from cruciferous vegetables or actinomycetes were screened in glioma cells (SHG-44, U87, and U251 cells) (Fig. 1a). Consequently, eight compounds (No. **32**, **90**, **91**, **106**, **113**, **124**, **126**, and **133** (LTr1), which are indicated in red points in Fig. 1b) decreased the viability of all three glioma cell lines by more than 50%, suggesting they possessed potential anti-glioma activity. Furthermore, the IC_{50} values of these compounds in glioma cells lines (Supplementary Table S1) and the levels of LDH secretion induced by these compounds (Supplementary Fig. S1) were measured, and the results confirmed their anti-glioma activities. Among these eight compounds, comprehensively considering their inhibitory effects on glioma cells and their toxic effects on normal astrocyte cells (Supplementary Fig. S2), LTr1 was selected as the lead compound. Notably, LTr1 had a higher IC_{50} value (4 μM) in mouse primary astrocytes and human SVG P12 normal astrocytes than glioma cells (1.97, 1.84, 2.03 μM against human SHG-44, U87, and U251 glioma cells, respectively). Moreover, glioma is a tumour of the central nervous system (CNS), and the ability of drugs to cross the blood-brain barrier should be emphasized. The log*P* and $logD^{7.4}$ of LTr1 were 4.96 and 2.11 (Fig. 1a), respectively, which indicated that LTr1 can cross the blood-brain barrier. Consequently, the LC-MS/MS analysis showed that the concentration of LTr1 in the brain was 3785.26 ± 898.90 ng/mL (~10.09 ± 2.40 μM) 3 h after the mice were administered 300 mg/kg by gavage and this value was higher than its IC_{50} against all the glioma cells, these results indicated that LTr1 could indeed cross the blood-brain barrier and exert its anti-glioma effect (Fig. 1c, d, Supplementary Fig. S3, and Supplementary Table S2).

LTr1 inhibited the proliferation of glioma cells by inducing S-phase arrest

To further assess the effects of LTr1 on glioma, the dose- and time-dependent effects of LTr1 on cell viability were studied in both SHG-44 and U87 cells. As expected, LTr1 inhibited the cell viability of the two glioma cell lines in a dose and time-dependent manner (Fig. 2a, b, and Supplementary Fig. S4). Furthermore, at the indicated concentrations, LTr1 inhibited the proliferation of glioma cells in a dose-dependent manner as shown by EdU assay and visualized under a fluorescence microscope (Fig. 2c and Supplementary Fig. S5e).

The inhibition of cell proliferation is often accompanied by cell cycle arrest. Therefore, the distribution of LTr1-treated glioma cells in different phases of the cell cycle was analyzed by propidium iodide (PI) staining. As shown in Fig. 2d, e, LTr1 significantly decreased the proportion of cells in the G_0/G_1 phase of the cell cycle, which was accompanied by an increased proportion of cells in the S-phase, in a dose-dependent manner. Correspondingly, the positive control drug PTX significantly increased the ratio of cells in the G_2/M phase [16]. It is well known that cyclin-dependent kinases (CDKs) are responsible for orchestrating the molecular events of orderly cell-cycle progression [17]. Therefore, the expression of CDKs in both glioma cell lines after treatment with LTr1 was measured using Western blotting. It was found that LTr1 down-regulated the expression of cyclin A2 and CDK2 to induce S-phase cell cycle arrest. In addition, LTr1 upregulated the expression of p21, which is a CDK inhibitor [18], whereas it exerted no significant effects on the expression of CDK4 which regulates the G_1 phase (Fig. 2f and Supplementary Fig. S5a–d). In addition, since DNA replication takes place in the S phase, DNA damage induces S phase arrest to inhibit cell proliferation [19]. Therefore, γ-H2AX, which is a marker of DNA damage, was used to assess DNA damage in glioma cells after exposure to LTr1. As expected, more γ-H2AX-positive cells, indicating the presence of DNA damage, were observed in the LTr1-treated group than in the control group (Supplementary Fig. S6). Collectively, LTr1 induced S phase cell cycle arrest by regulating cell-cycle-related proteins and causing DNA damage, resulting in the inhibition of glioma cell proliferation.

LTr1 induced glioma cells apoptosis by activating the mitochondrial intrinsic apoptotic pathway

The proliferation of cancer originates from its ability to avoid programmed cell death, which is called apoptosis [20]. Thus, the

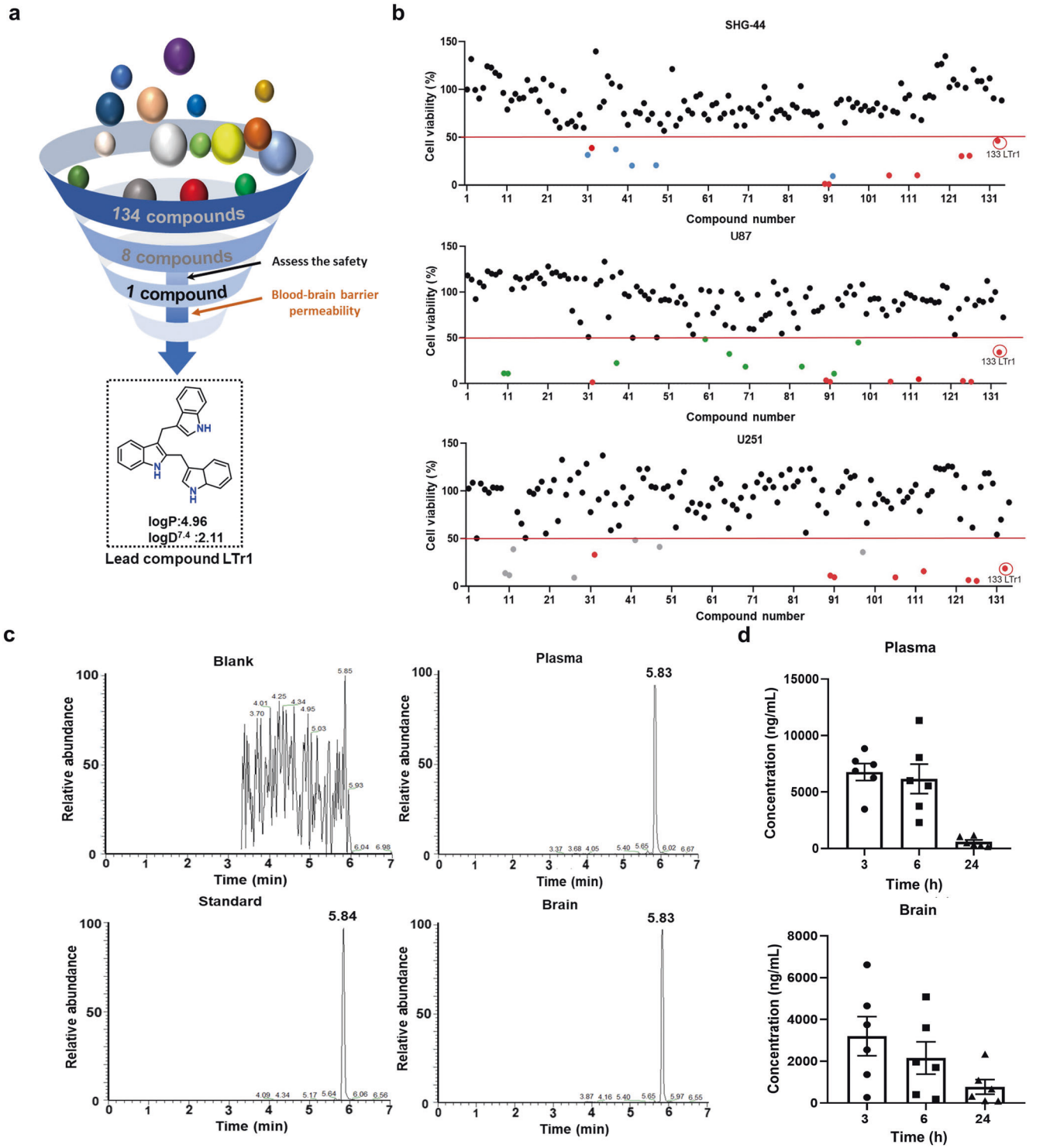

Fig. 1 Screening of lead compounds for anti-glioma activity. a Schematic diagram of screening lead compounds for anti-glioma activity. **b** Cell viabilities, examined by CCK-8 assay, after treatment of glioma cells including SHG-44, U87, and U251 with indicated compounds at 2 μM for 72 h, respectively. **c** HPLC profiles of LTr1 in brain tissues after oral intake of LTr1 (300 mg/kg). **d** Concentration of LTr1 in brain tissues and plasma at 3, 6, 24 h.

induction of apoptosis in cancer cells has been identified as an approach for the treatment of tumours. The morphological results of Hoechst 33342 staining showed different degrees of cell shrinkage, chromatin condensation, and nuclear fragmentation in glioma cells after treatment with various concentrations of LTr1 for 48 h (Fig. 3a and Supplementary Fig. S7a).

Furthermore, apoptotic cells were analyzed by the Annexin V-FITC/PI assay, and the proportion of apoptotic cells among glioma cells that were exposed to LTr1 was increased in a dose-dependent manner (Fig. 3b and Supplementary Fig. S7b). During apoptosis, internal or external stimuli initiates a series of highly controlled reactions, ultimately leading to cell death [21].

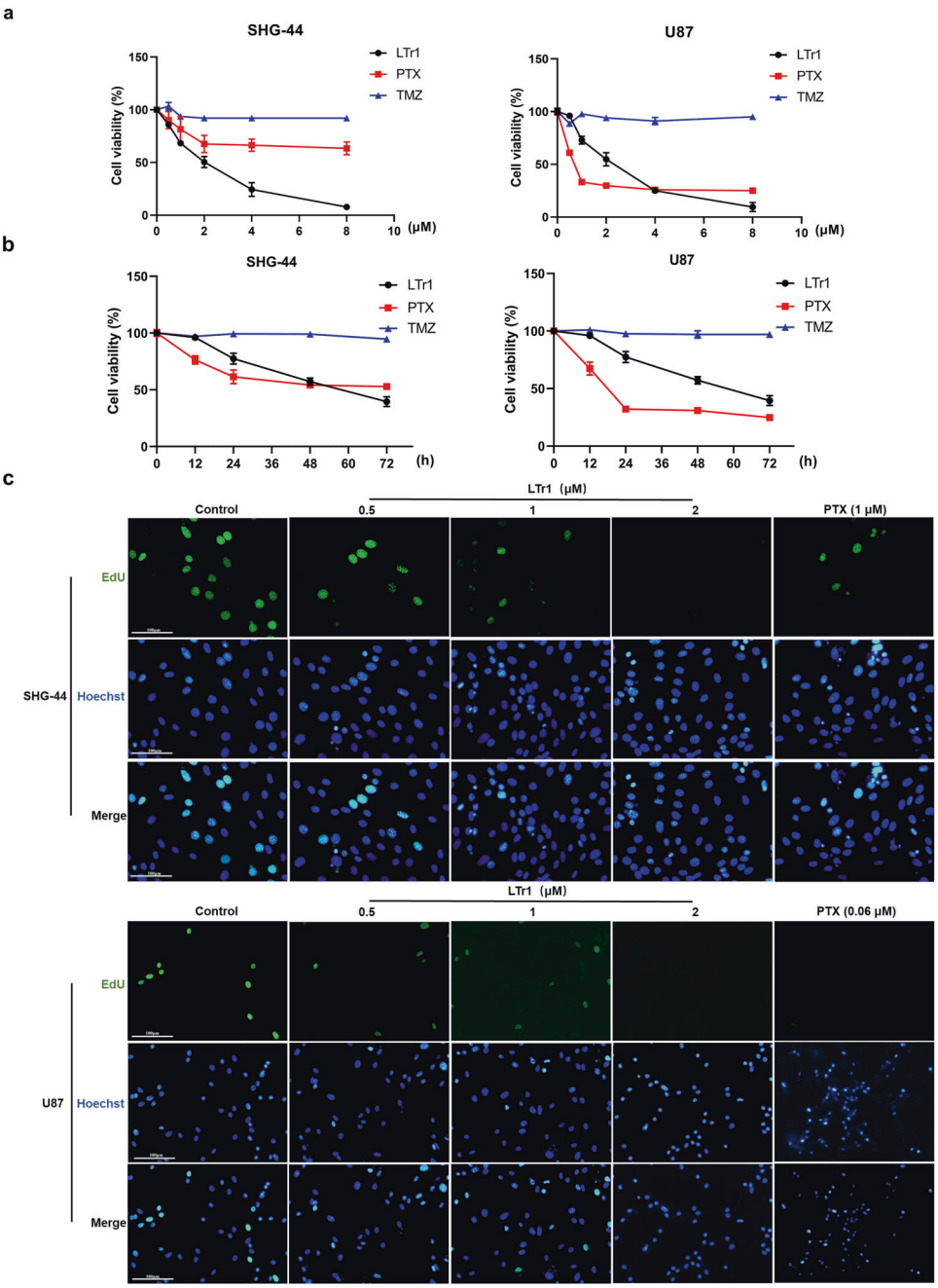

Fig. 2 (Continued).

Therefore, the expression of apoptosis-related proteins, especially proteins that are involved in the mitochondrial intrinsic apoptotic pathway, was measured. We found that LTr1 significantly increased the protein levels of cleaved caspase-3/9, Bax, and cytosol cytochrome *c* (cyto *c*), but decreased the levels of Bcl-2 and mitochondrial cyto *c* (Fig. 3c and Supplementary Fig. S7c–h), which demonstrated that LTr1 induced apoptosis by activating the intrinsic mitochondrial pathway.

LTr1 promoted ROS production and mitochondrial dysfunction in glioma cells

In cancers, the production of toxic levels of ROS exerts an anti-tumour effect via an increase in oxidative stress and induction of tumour cell death [22, 23]. Therefore, we determined whether ROS are involved in the LTr1-induced apoptosis of glioma cells. As shown in Fig. 4a–d, LTr1 significantly induced the intracellular ROS production in glioma cells assessed by H2DCF-DA staining, and the content of ROS in glioma cells increased rapidly as the concentration of LTr1 increased. In addition, we also found that LTr1 induced glioma cell apoptosis by activating mitochondrial pathways. Thus, the MitoSOX probe was used to measure the mitochondrial ROS levels in glioma cells. The results showed that LTr1 significantly induced the production of mitochondrial ROS in glioma cells (Fig. 4e–h). Furthermore, the mitochondrial membrane potential (MMP), which is another reliable indicator that is used to evaluate mitochondrial function, was analyzed with the fluorescent dye JC-1 [24]. The results showed that a considerable amount of the red JC-1 fluorescence was converted to green, indicating that the MMP of glioma cells was significantly decreased after exposure to different concentrations of LTr1

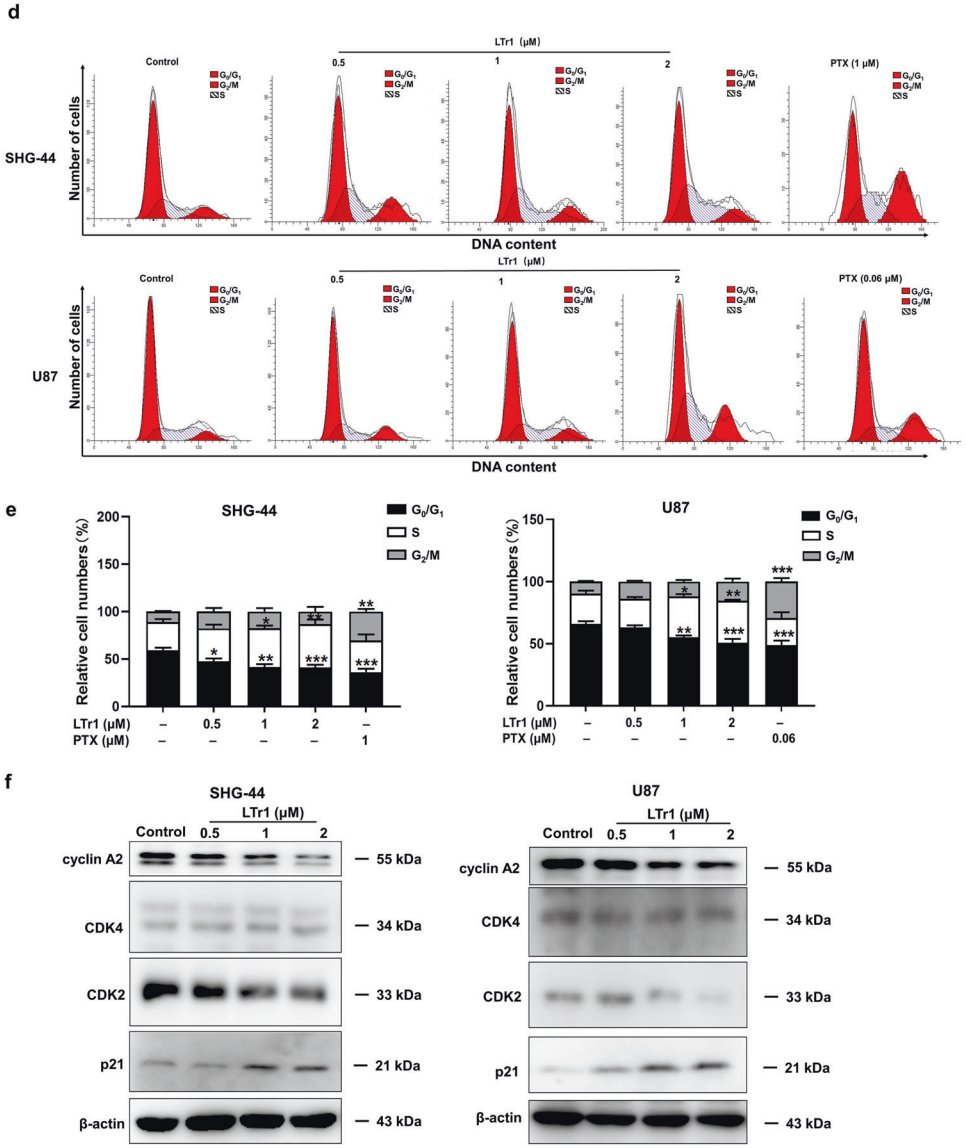

Fig. 2 LTr1 inhibited the proliferation of glioma cells via inducing S phase arrest. a SHG-44 and U87 were treated with LTr1 at the indicated concentrations for 48 h, and cell viability was detected by CCK-8 assay. **b** SHG-44 and U87 cells were treated with 2 μM LTr1 for 12, 24, 48, or 72 h, respectively. Cell viability was detected by CCK-8 assay. **c** The proliferation of glioma cells SHG-44 and U87 after treatment of LTr1 at indicated concentrations by EdU incorporation assay followed by visualization under a fluorescence microscope, compared with vehicle control (scale bar, 100 μm). **d**, **e** Glioma cells were stained with propidium iodide (PI), and cell cycle phase distribution was analyzed by flow cytometry. **f** Western blotting images of cell cycle-associated protein in glioma cells treated with LTr1. β-Actin was used as an internal control. Data are analyzed using two-way ANOVA. $^{*}P < 0.05$, $^{**}P < 0.01$ and $^{***}P < 0.001$ vs. control. Values are presented as means ± SEM from three or four independent experiments.

(Supplementary Fig. S8). These results suggested that LTr1 induced ROS production and mitochondrial dysfunction in glioma cells

TrkA was a potential target for glioma

TrkA is highly expressed in nervous tissues and is involved in the development of the central nervous system [25]. Various studies have reported that TrkA is related to the development of cancers [26]. According to the RNA-sequencing profiles of *NTRK1* of glioma patients and the corresponding clinical information from the TCGA dataset (https://www.cancer.gov/), we found that the *NTRK1* expression in glioma tissues was higher than that in normal control tissues ($P = 0.046$) (Fig. 5a), and high *NTRK1* expression was closely related to poor prognosis (Fig. 5b). To confirm the relationship between glioma and *NTRK1*, we performed the following experiments after transfecting the TrkA-targeting siRNA into glioma cells (Fig. 5c, d). After TrkA knockdown, the viability of glioma cells was significantly decreased, which was accompanied by increased LDH release (Fig. 5e, f). In addition, TrkA knockdown induced glioma cell apoptosis and inhibited glioma cell proliferation (Fig. 5g–j). These results showed that TrkA is associated with glioma and may be a potential target for the treatment of glioma.

LTr1 was a TrkA inhibitor

A series of indole alkaloids with indole and/or indole isostere motifs have been determined to be potent TrkA inhibitors (Supplementary Fig. S9) [27]. This finding encouraged us to evaluate the inhibitory effects of LTr1 on TrkA. To confirm whether inhibiting TrkA is effective for glioma treatment, the proliferation of SHG-44 and U87 glioma cells after treatment with LTr1 and the

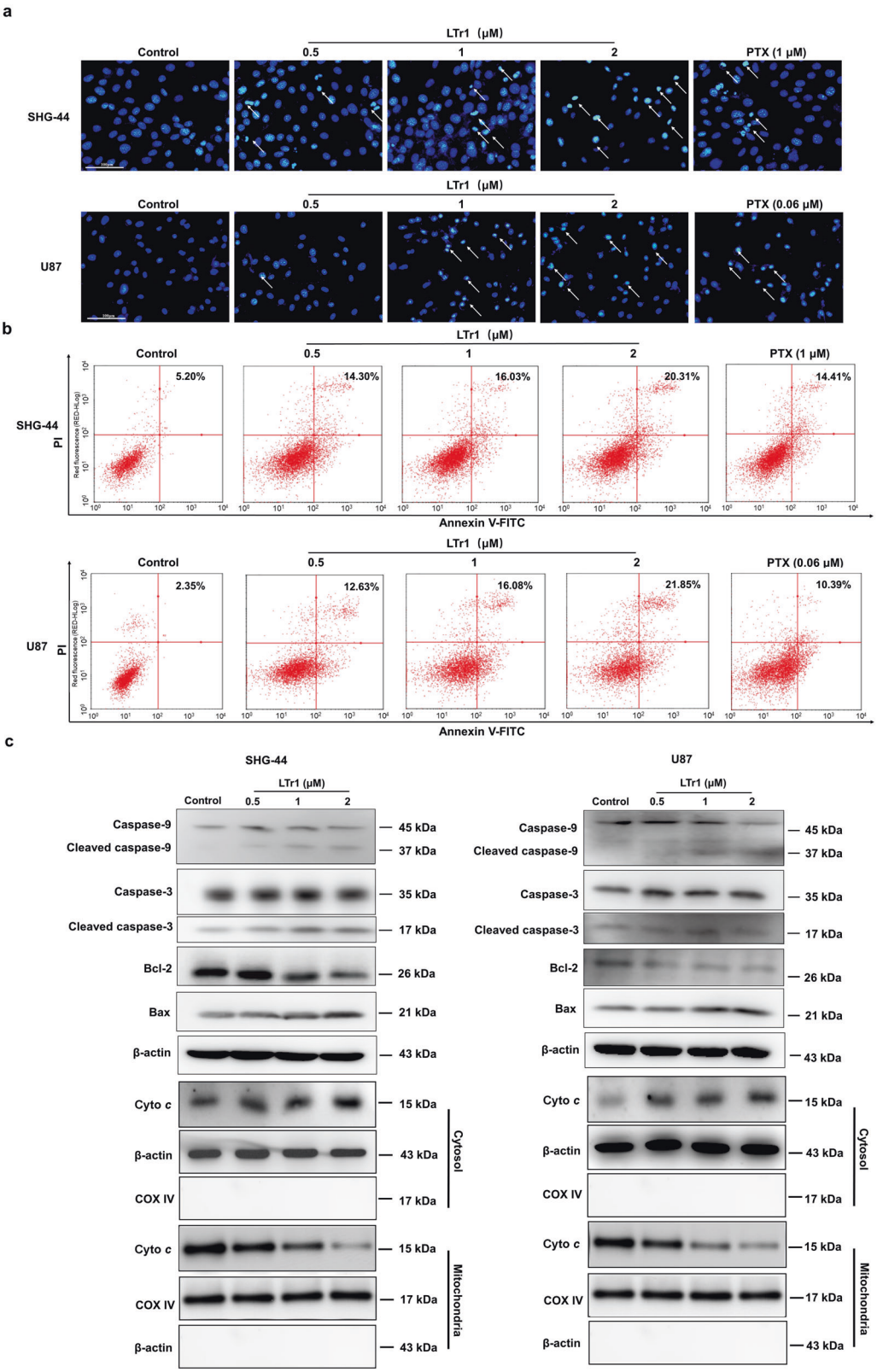

Fig. 3 LTr1 induced glioma cells apoptosis via activating the mitochondrial intrinsic apoptotic pathway. SHG-44 and U87 cells were treated with LTr1 (0.5, 1, 2 μM) and PTX (1 or 0.06 μM) for 48 h, respectively. **a**, **c** Apoptotic nuclear morphological changes were evaluated by Hoechst 33342 staining and observed under a fluorescence microscope. White arrows indicated chromatin condensation and nuclear fragmentation (scale bar, 100 μm). **c** The apoptosis-related proteins, including caspase-3/9, Bcl-2, Bax, and cyto *c* were analyzed by Western blotting. β-Actin or COX IV was used as an internal control. Data are analyzed using One-way ANOVA. $^{*}P < 0.05$, $^{**}P < 0.01$, and $^{***}P < 0.001$ vs. control. Values are presented as means ± SEM from three or four independent experiments.

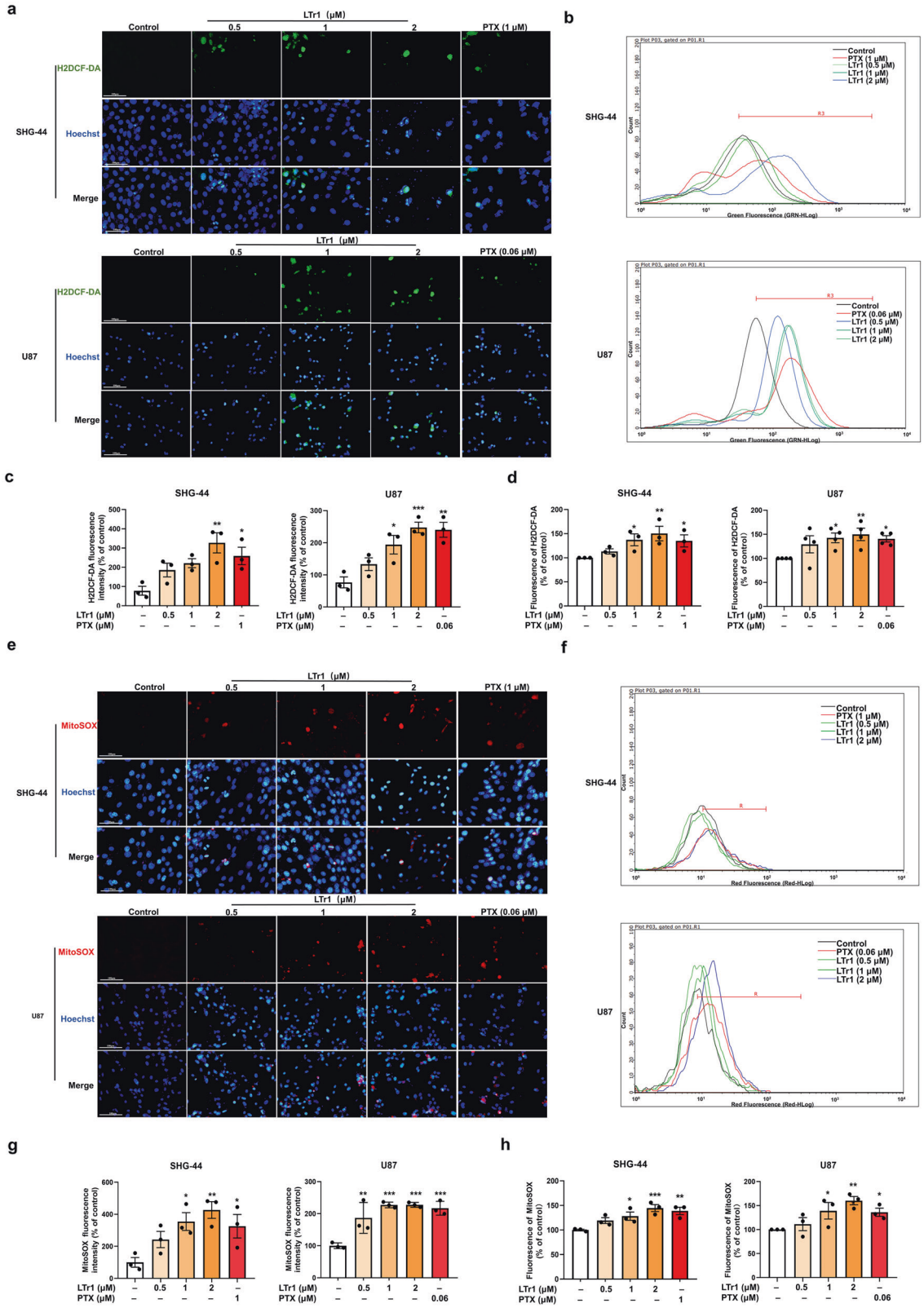

Fig. 4 LTr1 induced oxidative damage in glioma cells. SHG-44 and U87 cells were treated with the indicated concentrations of LTr1 and PTX for 48 h. They were loaded with H2DCF-DA and MitoSOX probe for 30 min, followed by observing under a fluorescence microscope (scale bar, 100 μm) (**a**, **e**) or analyzing via flow cytometer (**b** and **f**). **c**, **d**, and **g**, **h** Statistical analysis of H2DCF-DA and MitoSOX, respectively. Data are analyzed using One-way ANOVA. $^{*}P < 0.05$, $^{**}P < 0.01$ and $^{***}P < 0.001$ vs. control group. Values are presented as means ± SEM from three or four independent experiments.

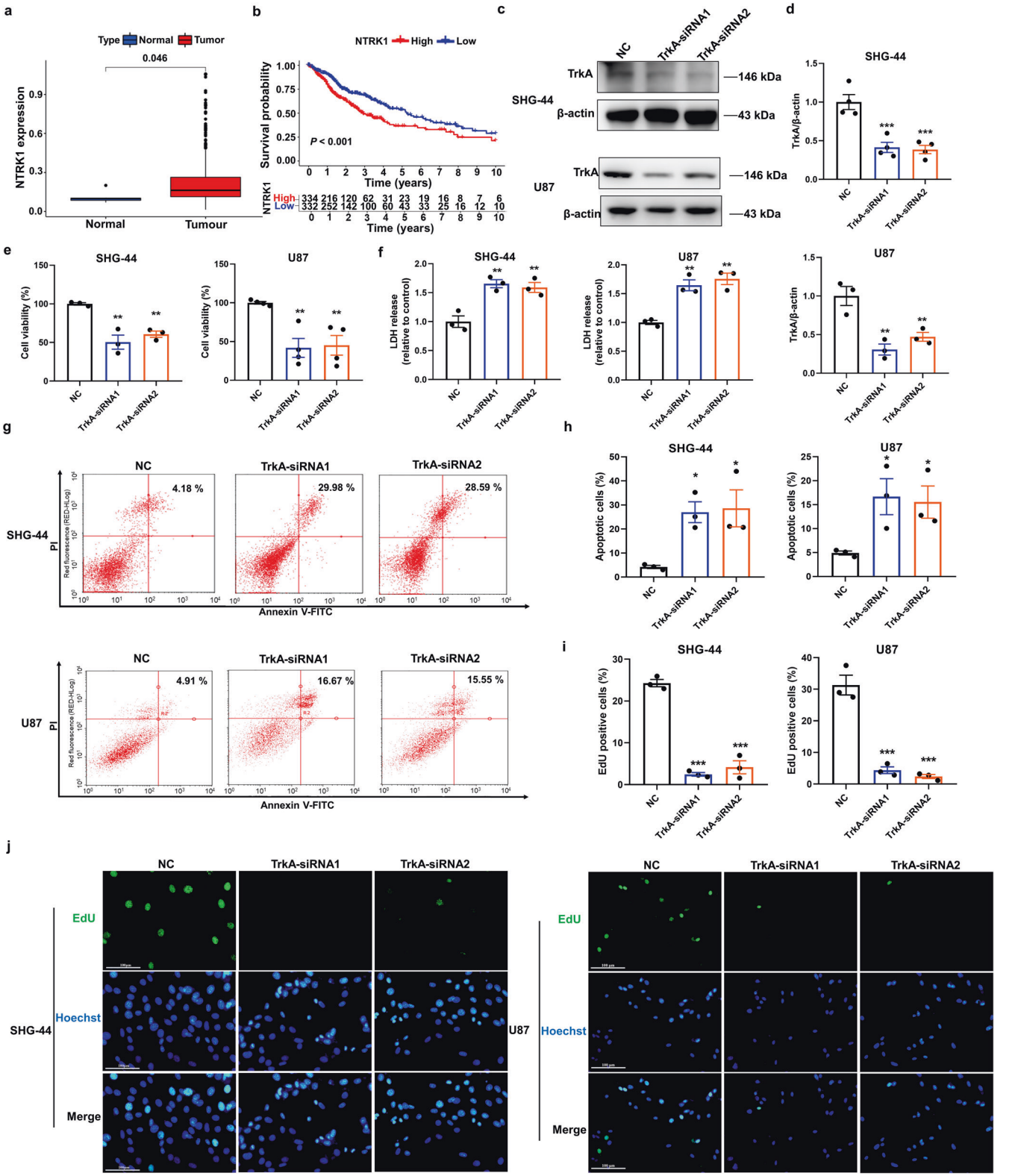

Fig. 5 TrkA was a potential target for glioma. All samples with *NTRK1* expression data across all patient characteristics were analyzed from TCGA database (https://www.cancer.gov/). **a** Expression levels of *NTRK1* in glioma tissues ($n = 698$) are significantly higher than those in adjacent normal tissues ($n = 5$). The lines within boxes are medians, and the whiskers are the minimal and maximal values. **b** High expression of *NTRK1* correlates with poor overall survival of glioma patients in TCGA cohort. SHG-44 and U87 cells were cultured and transfected with siRNA targeting the mRNA encoding TrkA or empty vector for 48 h. All of the data of knockdown (KD) cells in **c–j** were compared with the negative control (NC) both in SHG-44 and U87 cell lines. **c**, **d** Expression of TrkA was analyzed by Western blotting. **e** The cell viabilities were analyzed by CCK-8 assay. **f** The levels of LDH release were determined by LDH assay kit. **g**, **h** Cells were stained by Annexin V-FITC and PI and analyzed by flow cytometry. **i**, **j** The proliferation of glioma cells was measured by EdU assay kit and observed under a fluorescence microscope (scale bar, 100 μm). Data are analyzed using One-way ANOVA. $^{*}P < 0.05$, $^{**}P < 0.01$ and $^{***}P < 0.001$ vs. NC group. Values are presented as means ± SEM from three or four independent experiments.

positive control LOXO-101, which is a TrkA inhibitor [28], was analyzed. As expected, both LTr1 and LOXO-101 significantly inhibited the cell viability and induced the LDH release of the two glioma cell lines (Fig. 6a and Supplementary Fig. S10a). In addition to the increase in apoptotic cell numbers, the proliferation was decreased compared with that in the control group (Fig. 6b, c, and Supplementary Fig. S10b, c). These results suggested that TrkA is a potential target for glioma therapy, and LTr1 may exert an anti-glioma effect by inhibiting TrkA activity.

To confirm that LTr1 is a TrkA inhibitor, enzyme inhibition, molecular docking analysis, MST, and BLI analyses were performed. As a result, LTr1 was found to inhibit TrkA kinase activity ($IC_{50} = 3.20$ μM) (Fig. 6d). NGF, which is the positive control ligand of TrkA, was used to confirm the effectiveness of the MST assay (Supplementary Fig. S11) and LTr1 was demonstrated to bind to TrkA with a dissociation constant of 14.16 μM (Fig. 6e). BLI kinetics analysis showed that the affinity (K_D) for TrkA was 9.7 μM (Supplementary Fig. S12).

Then, we performed a molecular docking analysis to investigate the binding site for TrkA/LTr1 complex formation based on the published crystal structure of human TrkA (PDB ID: 6d20). According to molecular docking (MD) simulations, the binding free energy between LTr1 and TrkA was calculated to be −6.32 kcal/mol. The corresponding docking conformation suggested that LTr1 fits into the active pocket, forming multiple meaningful interactions with surrounding amino acid residues, including Ile572, Leu641, Leu567, Leu564, Gly667, Leu486, Gly670, Ser484, Gly485, His648 and Phe646, and this pocket mainly provides a suitable hydrophobic environment for binding. We also observed three hydrogen bonds that formed between the NH moieties of LTr1 and the backbone carboxyl oxygen atom of the amino acid residues Glu560 and Asp668 and the primary chain carbonyl oxygen atom of the amino acid residue Ile666. In addition, a π-σ interaction between the pyrrole ring of LTr1 and Lys544 residue was observed (Fig. 6f). Altogether, these experiments corroborated the robust binding of LTr1 with TrkA (Fig. 6e, f, and Supplementary Fig. S12).

Additionally, 2 μM LTr1 significantly decreased the protein levels of TrkA in both the SHG-44 and U87 cell lines (Fig. 6g and Supplementary Fig. S13a). Furthermore, this treatment suppressed the phosphorylation of some downstream regulatory targets of TrkA such as the PI3K/AKT pathway (Fig. 6h and Supplementary Fig. S13b, c) [29].

To verify that LTr1 induced glioma cell apoptosis and inhibited glioma cells proliferation via TrkA, apoptosis rate and viability were analyzed after TrkA-siRNA-transfected with in SHG-44 and U87 cells were treated with LTr1 (Supplementary Fig. S14). The results showed that LTr1-mediated inhibition of proliferation was abolished after transfection of glioma cells with TrkA-siRNA, suggesting that TrkA was the main target of LTr1.

LTr1 inhibited the tumour growth and induced cells apoptosis in vivo

To evaluate the efficacy of LTr1 in vivo, we compared its effects to those of PTX using a U87 xenograft nude mouse model (Fig. 7a) [30]. As shown in Fig. 7b–d, 300 mg/kg LTr1 significantly inhibited tumour growth compared with the blank control and vehicle administration control. The average tumour weight decreased from 1.29 ± 0.40 g (control group) to 0.58 ± 0.20 g (LTr1 group, 300 mg/kg dose), with an inhibition rate of 54.71% compared with the blank control group. Moreover, no significant weight loss or any other obvious signs of toxicity was observed in the livers, spleens, or kidneys after LTr1 administration (Supplementary Fig. S15). As shown in Fig. 7e and Supplementary Fig. S16, tumours in the vehicle control group exhibited strong staining for Ki67. In contrast, those from the LTr1-treated groups (300 mg/kg dose) showed significantly fewer Ki67-positive cells. Furthermore, cell cavitation and chromatin condensation were analyzed to assess apoptosis and the inhibition of proliferation, and these responses were observed in tumour tissues from the 300 mg/kg LTr1-treated groups. Similarly, the TUNEL staining assay showed an apparent increase in apoptotic cells compared to the vehicle control (Fig. 7f).

Considering that glioma is a tumour of CNS and the influence of the BBB, we further established an orthotopic xenograft glioma model to evaluate the effect of LTr1 (Fig. 8a). The NMR imaging results showed that LTr1 significantly decreased the proliferation of glioma cells compared with the vehicle without changing the mouse body weights (Fig. 8b, c). LTr1 also inhibited the liver metastasis of tumours (Fig. 8d and Supplementary Fig. S17).

DISCUSSION

Cruciferous vegetables, including cabbage, broccoli, and radish, are rich sources of isothiocyanates and I3C, which are well known for their protective effects against cancer [31]. In our search for a potent agent that could be used for glioma treatment, we found that LTr1, which is a compound that is derived from cruciferous vegetables, exerted anti-glioma effects by inhibiting proliferation and inducing cell apoptosis. Our study suggested that LTr1 could cross the blood-brain barrier. This is the first time that the concentration and distribution of LTr1 has been confirmed in mice after its administration, and the results provided direct evidence that LTr1 could directly cross the blood-brain barrier. Although LTr1 exerts inferior in anti-tumour effects than PTX in the U87 xenograft model, we cannot neglect the side effects of PTX, such as hepatotoxicity observed in our experiments, which was consistent with a previous study [32], and peripheral neuropathy, hypersensitivity, haemolysis and so on [33–35]. In addition, the resistance to PTX treatment is a substantial obstacle to its clinical applications and one of the significant causes of death associated with treatment failure. LTr1, which is derived from cruciferous vegetables that are consumed daily and are inexpensive but rich sources of nutrients, caused less toxicity than PTX (Supplementary Fig. S13), and it prolongs the survival time of patients with tumour-bearing. We think LTr1 could be a lead compound for tumour treatment that meet the clinical demands of safety, low cost, and easy access.

TrkA (encoded by the gene *NTRK1*) is widely expressed and involved in the development of the CNS [36]. TrkA modulates cell proliferation, differentiation, metabolism, and even apoptosis through the MAPK pathway [37]. However, if it is activated by *NTRK1* gene fusions, mutations, splice variant formation, and overexpression, it causes a high risk of carcinogenesis [38–40]. Therefore, inhibition of TrkA is recognized as a potential target for tumour therapy. It had been reported that TrkA exerts an anti-tumour effect by inducing cell apoptosis and cell cycle arrest. The TrkA kinase inhibitor KRC-108 was reported to induce cell apoptosis and G_1 phase cell cycle arrest by suppressing the phosphorylation of Akt and ERK1/2 in colon cancer. Another TrkA inhibitor, namely R234 exerts caspase3/7-independent apoptotic effects by inhibiting the PI3K/AKT/mTOR pathway in glioblastoma [41–44]. In our study, we confirmed that TrkA is overexpressed in the glioma and its overexpression associated with the development of glioma, making it a potential therapeutic target for glioma.

This study showed for the first time that LTr1 directly binds to TrkA to inhibit its kinase activity and the downstream PI3K/AKT pathway. In addition, the induction of glioma apoptosis and inhibition of proliferation by LTr1 requires TrkA. Therefore, we believe that TrkA is a potential therapeutic target for glioma due to its anti-glioma effects. Interestingly, we found that LTr1 induced DNA damage in glioma cells, with different levels of damage observed in SHG-44 and U87 cells (Supplementary Fig. S6). It was widely known that gliomas are heterogeneous [45]. Although SHG-44 and U87 cells are glioma cell lines; their sources and genetic backgrounds are different. According to the ATCC website

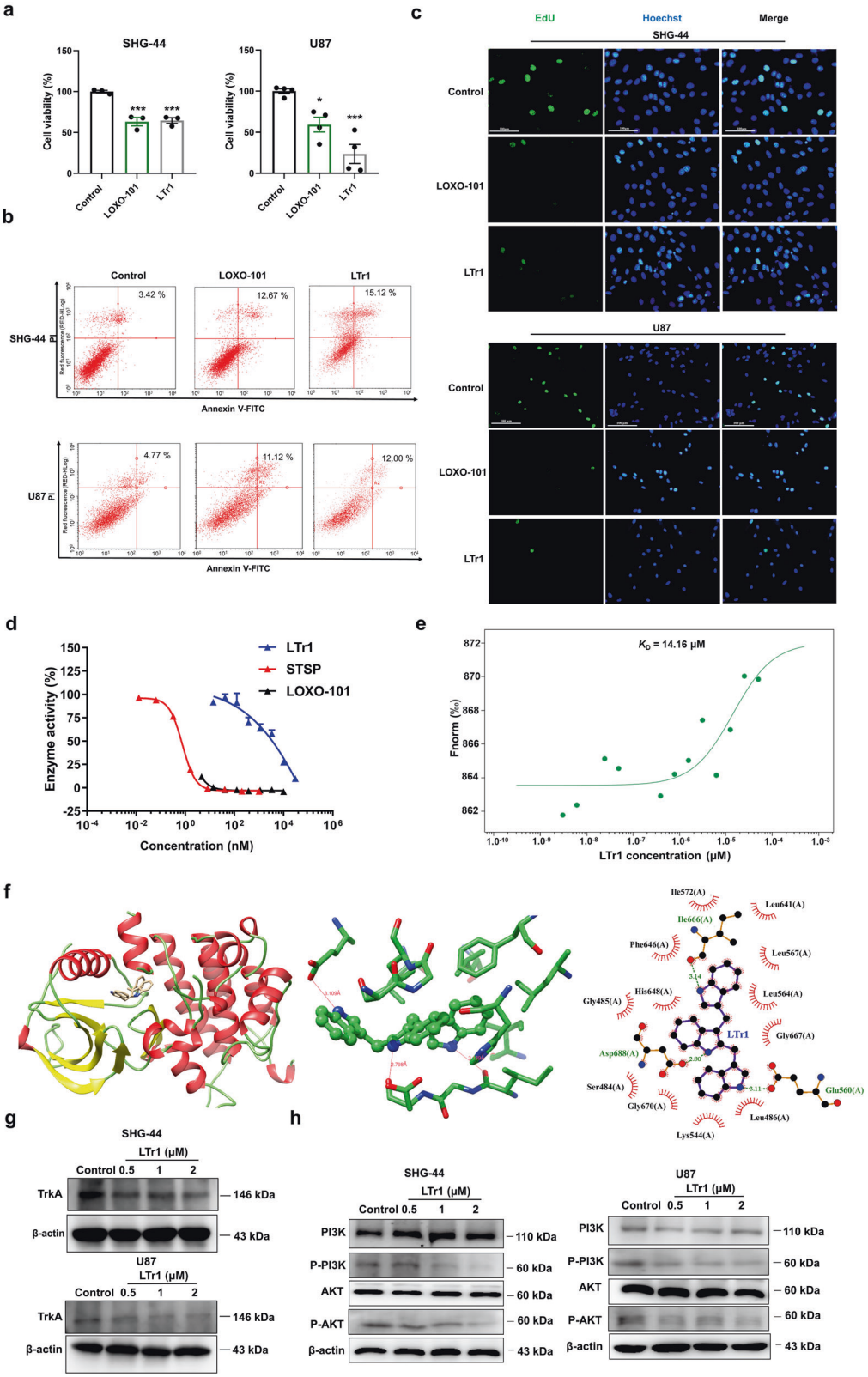

Fig. 6 LTr1 was a TrkA inhibitor. SHG-44 and U87 cells were treated with TrkA inhibitor LOXO-101 (1 μM) and LTr1 (2 μM) for 48 h. **a** Cell viability was analyzed by CCK-8 assay. **b** Cells were stained by Annexin V-FITC and PI, and analyzed by flow cytometry. **c** The proliferation profiles of glioma cells were assayed by an EdU assay kit and observed under a fluorescence microscope (scale bar, 100 μm). **d** In vitro inhibition of TrkA by LTr1, with STSP and LOXO-101 as positive controls. **e** The K_D value of LTr1 binding to TrkA was determined by microscale thermophoresis (MST) to be 14.16 μM. **f** Computational predicted binding mode of LTr1 with TrkA. Key amino acid residues involved in the binding of LTr1 in the active pocket of human TrkA, identified by Gibbs binding free energy calculations within AMBER software. **g**, **h** SHG-44, and U87 cells were treated with the indicated concentrations of LTr1 for 48 h, and protein levels of TrkA and PI3K/AKT were performed by Western blotting. β-Actin was an internal control. Data are analyzed using One-way ANOVA. $^{*}P < 0.05$, $^{**}P < 0.01$ and $^{***}P < 0.001$ vs. control. Values are presented as means ± SEM from three or four independent experiments.

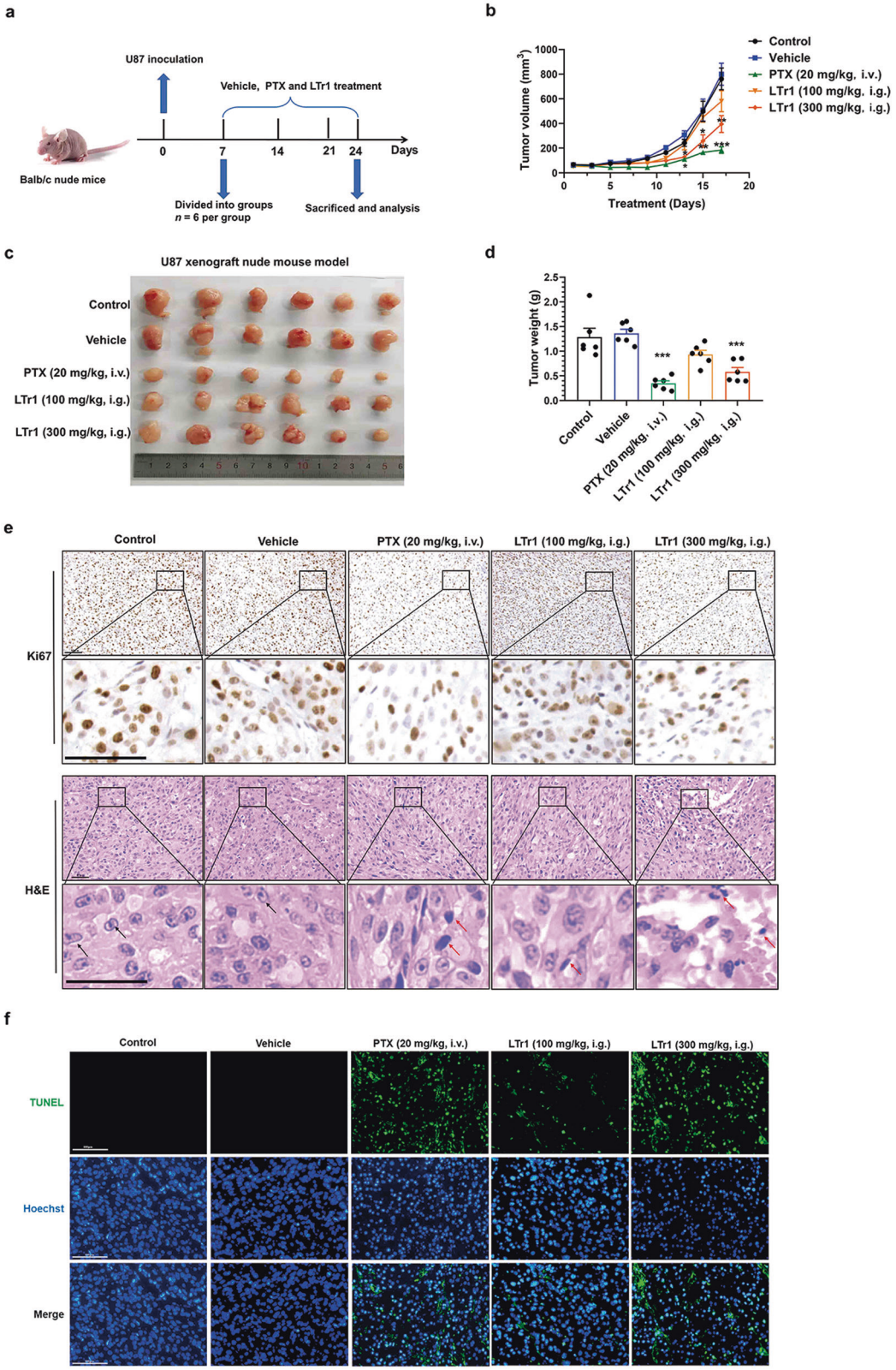

Fig. 7 LTr1 inhibited tumour growth and induced cell apoptosis in U87- subcutaneously heterotopic xenografted nude mice. **a** Experimental design using 4-week-old female nude mice randomized into five groups ($n = 6$). **b**, **c** The anti-tumour activity was evidenced from the tumour volume. **d** Final mean tumour weights for U87 tumours in the five experimental groups. **e** Representative H&E staining images and Ki67 immunostaining in U87-xenograft tumours (scale bar, 40 μm). Black and red arrows indicated live and apoptotic cells, respectively. **f** TUNEL staining of U87-xenografted tumours (scale bar, 100 μm). Data are analyzed using One-way ANOVA. $^{*}P < 0.05$, $^{**}P < 0.01$ and $^{***}P < 0.001$ vs. control. Values are presented as means ± SEM. $n = 6$ mice per group.

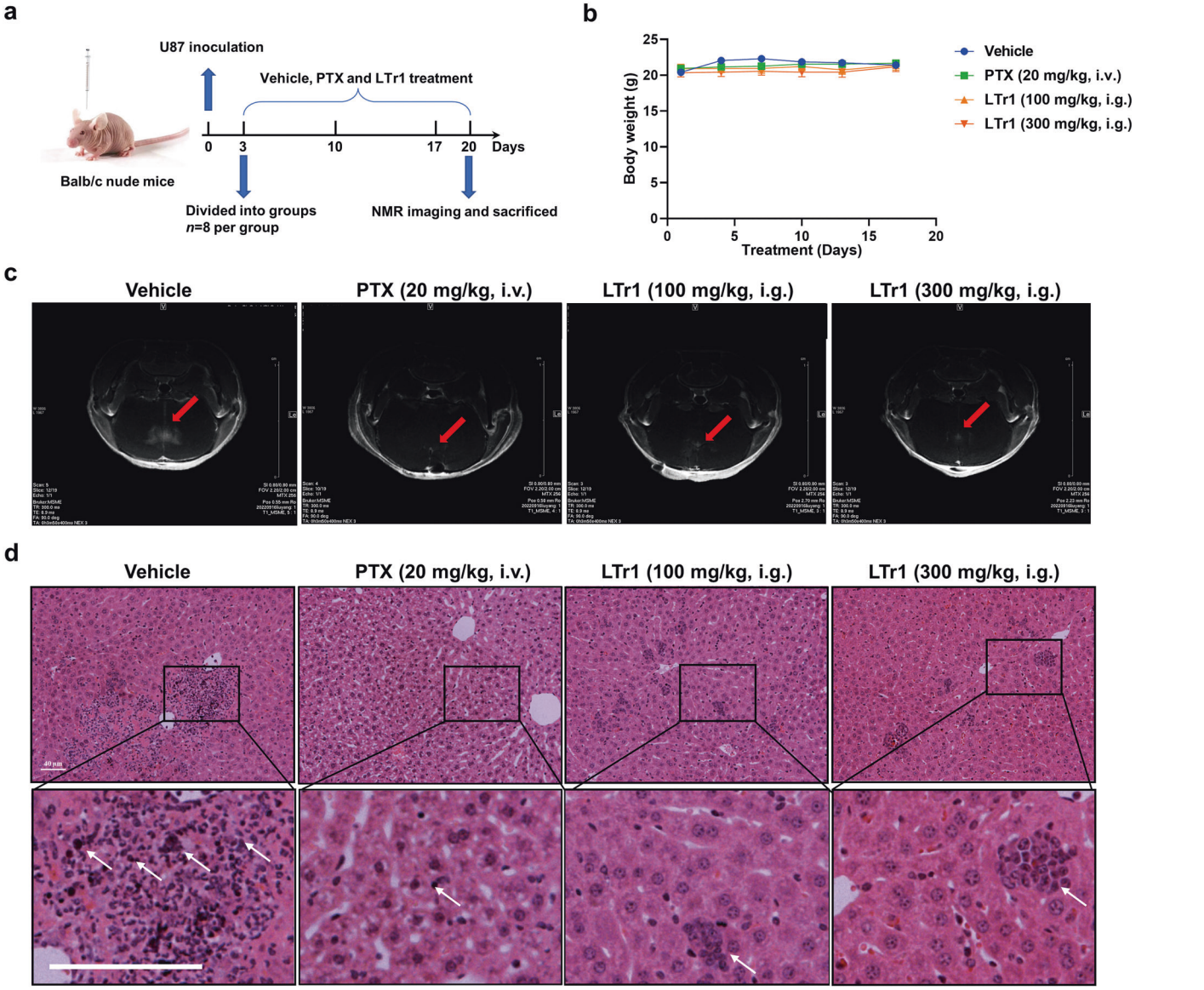

Fig. 8 LTr1 inhibited the growth and metastasis of tumour in U87 orthotopic xenograft model. a Experimental design using 4-week-old female nude mice was randomized into four groups ($n = 6$). **b** Body weight variation of mice during the experimental period. **c** Representative NMR imaging of tumour. **d** Representative H&E staining of the liver. White arrows indicated the metastasis of tumour. Scar bars, 40 μm. $n = 6$ mice per group.

(https://www.atcc.org/) and previous studies, SHG-44 cells were derived from a grade 2–3 anterior lymph node astrocytoma, and U87 cells were derived from glioblastoma of the brain [4, 46]. In addition, SHG-44 cells were derived from a female patient, while U87 cells were derived from a male patient. Apart from differences in sex, differences in the race and age of patients may also cause differences in the effects of LTr1. The difference described above could suggest that these two cell lines may have different sensitivities to LTr1. Additionally, TrkA is a member of the tropomyosin receptor kinase (TRK) family and is highly conserved, it has a structure that is similar to that of TrkB and TrkC, which are the other two members of the TRK family [47]. Therefore, whether LTr1 can affect TrkB/C, needs to be further confirmed.

In summary, LTr1 was screened from 134 natural compounds and shown for the first time to be a promising lead compound for glioma treatment. LTr1 can cross the blood-brain barrier, thus inhibiting the progression of glioma, and induces cell apoptosis via directly binding to TrkA to inhibit its kinase activity and the downstream PI3K/AKT pathway. Our study provides a new insight into the benefit of consuming cruciferous vegetables and indicates the potential role of LTr1 in the treatment of glioma.

ACKNOWLEDGEMENTS

This research was supported by grants from the National Key R&D Program of China (Nos. 2021ZD0202901 and 2018YFC1706205), and the National Natural Science Foundation of China (Nos. 81991523 and 82073721). We thank the Experiment Center for Science and Technology, Nanjing University of Chinese Medicine, for providing the instrumentation.

AUTHOR CONTRIBUTIONS

GH, RXT, and YL designed the experiments. QQS, LPL, JCQ, YLC, KW, and JWS performed the experiments. QQS, LPL, and YL analyzed and interpreted the data from experiments. JHD provided technical support. QQS wrote the manuscript. YL, ML, and LPL made critical modifications to the manuscript. All authors read and approved the final manuscript.

ADDITIONAL INFORMATION

Supplementary information The online version contains supplementary material available at https://doi.org/10.1038/s41401-022-01033-y.

Competing interests: The authors declare no competing interests.

REFERENCES

1. Baky MH, Shamma SN, Xiao J, Farag MA. Comparative aroma and nutrients profiling in six edible versus nonedible cruciferous vegetables using ms based metabolomics. Food Chem. 2022;383:132374.
2. Ahmed AG, Hussein UK, Ahmed AE, Kim KM, Mahmoud HM, Hammouda O, et al. Mustard seed (*Brassica nigra*) extract exhibits antiproliferative effect against human lung cancer cells through differential regulation of apoptosis, cell cycle, migration, and invasion. Molecules. 2020;25:2069.
3. Lenting K, Verhaak R, Ter Laan M, Wesseling P, Leenders W. Glioma: Experimental models and reality. Acta Neuropathol. 2017;133:263–82.
4. Yang K, Wu Z, Zhang H, Zhang N, Wu W, Wang Z, et al. Glioma targeted therapy: Insight into future of molecular approaches. Mol Cancer. 2022;21:39.
5. Lapointe S, Perry A, Butowski NA. Primary brain tumours in adults. Lancet. 2018;392:432–46.
6. Zhu WJ, Lin LP, Liu D, Qian JC, Zhou BB, Yuan DD, et al. Pharmacophore-inspired discovery of FLT3 inhibitor from kimchi. Food Chem. 2021;361:130139.
7. Lin LP, Liu D, Qian JC, Wu L, Zhao Q, Tan RX. Post-ingestion conversion of dietary indoles into anticancer agents. Natl Sci Rev. 2022;9:nwab144.
8. Thomson CA, Ho E, Strom MB. Chemopreventive properties of 3,3′-diindolylmethane in breast cancer: Evidence from experimental and human studies. Nutr Rev. 2016;74:432–43.
9. Yerushalmi R, Bargil S, Ber Y, Ozlavo R, Sivan T, Rapson Y, et al. 3,3-Diindolylmethane (DIM): A nutritional intervention and its impact on breast density in healthy BRCA carriers. A prospective clinical trial. Carcinogenesis. 2020;41:1395–401.
10. Liu X, Zhao P, Wang X, Wang L, Zhu Y, Song Y, et al. Celastrol mediates autophagy and apoptosis via the ROS/JNK and AKT/mTOR signaling pathways in glioma cells. J Exp Clin Cancer Res. 2019;38:184.
11. Ding Y, Zhou Y, Li Z, Zhang H, Yang Y, Qin H, et al. Oroxylin a reversed fibronectin-induced glioma insensitivity to temozolomide by suppressing IP_3R1/Akt/β-catenin pathway. Life Sci. 2020;260:118411.
12. Yan Y, Liu X, Gao J, Wu Y, Li Y. Inhibition of TGF-β signaling in gliomas by the flavonoid diosmetin isolated from *Dracocephalum peregrinum* l. Molecules. 2020;25:192.
13. Jong L, Jiang F, Li G, Mortelmans K. Analogs of indole-3-carbinol and their use as agents against infection. US patent 20080097816P. 2010 Mar 25.
14. Bagal SK, Omoto K, Blakemore DC, Bungay PJ, Bilsland JG, Clarke PJ, et al. Discovery of allosteric, potent, subtype selective, and peripherally restricted TRKA kinase inhibitors. J Med Chem. 2019;62:247–65.
15. Morris GM, Huey R, Lindstrom W, Sanner MF, Belew RK, Goodsell DS, et al. AutoDock4 and AutoDockTools4: Automated docking with selective receptor flexibility. J Comput Chem. 2009;30:2785–91.
16. Son KH, Kim MY, Shin JY, Kim JO, Kang JH. Synergistic antitumor effect of taxanes and CDK4/6 inhibitor in lung cancer cells and mice harboring KRAS mutations. Anticancer Res. 2021;41:4807–20.
17. Ingham M, Schwartz GK. Cell-cycle therapeutics come of age. J Clin Oncol. 2017;35:2949–59.
18. Yadav V, Varshney P, Sultana S, Yadav J, Saini N. Moxifloxacin and ciprofloxacin induces s-phase arrest and augments apoptotic effects of cisplatin in human pancreatic cancer cells via erk activation. BMC Cancer. 2015;15:581.
19. Huang RX, Zhou PK. DNA damage response signaling pathways and targets for radiotherapy sensitization in cancer. Signal Transduct Target Ther. 2020;5:60.
20. Reed JC. Dysregulation of apoptosis in cancer. J Clin Oncol. 1999;17:2941–53.
21. Grilo AL, Mantalaris A. Apoptosis: A mammalian cell bioprocessing perspective. Biotechnol Adv. 2019;37:459–75.
22. Ren B, Cai ZC, Zhao XJ, Li LS, Zhao MX. Evaluation of the biological activity of folic acid-modified paclitaxel-loaded gold nanoparticles. Int J Nanomed. 2021;16:7023–33.
23. Yang C, Li Y, Hu W, Wang X, Hu J, Yuan C, et al. Teoa promotes autophagic cell death via ros-mediated inhibition of mTOR/p70s6k signaling pathway in pancreatic cancer cells. Front Cell Dev Biol. 2021;9:734818.
24. Elefantova K, Lakatos B, Kubickova J, Sulova Z, Breier A. Detection of the mitochondrial membrane potential by the cationic dye JC-1 in l1210 cells with massive overexpression of the plasma membrane abcb1 drug transporter. Int J Mol Sci. 2018;19:1985.
25. Wang Y, Long P, Wang Y, Ma W. Ntrk fusions and TRK inhibitors: Potential targeted therapies for adult glioblastoma. Front Oncol. 2020;10:593578.
26. Gambella A, Senetta R, Collemi G, Vallero SG, Monticelli M, Cofano F, et al. Ntrk fusions in central nervous system tumors: A rare, but worthy target. Int J Mol Sci. 2020;21:753.
27. Jiang T, Wang G, Liu Y, Feng L, Wang M, Liu J, et al. Development of small-molecule tropomyosin receptor kinase (Trk) inhibitors for ntrk fusion cancers. Acta Pharm Sin B. 2021;11:355–72.
28. Umezawa K, Lin Y. Inhibition of matrix metalloproteinase expression and cellular invasion by NF-κb inhibitors of microbial origin. Biochim Biophys Acta Proteins Proteom. 2020;1868:140412.
29. Conroy JN, Coulson EJ. High-affinity trka and p75 neurotrophin receptor complexes: A twisted affair. J Biol Chem. 2022;298:101568.
30. Wang H, Wang S, Wang R, Wang X, Jiang K, Xie C, et al. Co-delivery of paclitaxel and melittin by glycopeptide-modified lipodisks for synergistic anti-glioma therapy. Nanoscale. 2019;11:13069–77.
31. Mori N, Shimazu T, Sasazuki S, Nozue M, Mutoh M, Sawada N, et al. Cruciferous vegetable intake is inversely associated with lung cancer risk among current nonsmoking men in the japan public health center (jphc) study. J Nutr. 2017;147:841–9.
32. Gur C, Kandemir FM, Caglayan C, Satıcı E. Chemopreventive effects of hesperidin against paclitaxel-induced hepatotoxicity and nephrotoxicity via amendment of Nrf2/Ho-1 and caspase-3/Bax/Bcl-2 signaling pathways. Chem-Biol Interact. 2022;365:110073.
33. Halámková J, Adámková Krákorová D, Demlová R. Anisocoria as a side effect of paclitaxel treatment. Klinicka Onkol: Cas Ceske a Slovenske onkologicke spolecnosti. 2021;34:306–8.
34. Abu Samaan TM, Samec M, Liskova A, Kubatka P, Büsselberg D. Paclitaxel's mechanistic and clinical effects on breast cancer. Biomolecules. 2019;9:789:1–22.
35. Gu W, Chen J, Patra P, Yang X, Gu Q, Wei L, et al. Nanoformulated water-soluble paclitaxel to enhance drug efficacy and reduce hemolysis side effect. J Biomater Appl. 2017;32:66–73.
36. Siozopoulou V, Smits E, De Winne K, Marcq E, Pauwels P. Ntrk fusions in sarcomas: Diagnostic challenges and clinical aspects. Diagnostics. 2021;11:478.
37. Nakagawara A. Trk receptor tyrosine kinases: A bridge between cancer and neural development. Cancer Lett. 2001;169:107–14.
38. Xu C, Ge S, Cheng J, Gao H, Zhang F, Han A. Pathological and prognostic characterization of craniopharyngioma based on the expression of TrkA, β-catenin, cell cycle markers, and BRAF V600E mutation. Front Endocrinol. 2022;13:859381.
39. Lagadec C, Meignan S, Adriaenssens E, Foveau B, Vanhecke E, Romon R, et al. TrkA overexpression enhances growth and metastasis of breast cancer cells. Oncogene. 2009;28:1960–70.
40. Miranda C, Mazzoni M, Sensi M, Pierotti MA, Greco A. Functional characterization of NTRK1 mutations identified in melanoma. Genes Chromosomes Cancer. 2014;53:875–80.
41. Oh TI, Lee YM, Nam TJ, Ko YS, Mah S, Kim J, et al. Fascaplysin exerts anti-cancer effects through the downregulation of survivin and HIF-1α and inhibition of VEGFR2 and TRKA. Int J Mol Sci. 2017;18:2074.
42. Wu T, Qin Q, Lv R, Liu N, Yin W, Hao C, et al. Discovery of quinazoline derivatives CZw-124 as a pan-TRK inhibitor with potent anticancer effects in vitro and in vivo. Eur J Med Chem. 2022;238:114451.
43. Lee HJ, Moon Y, Choi J, Heo JD, Kim S, Nallapaneni HK, et al. Characterization of KRC-108 as a TrkA kinase inhibitor with anti-tumor effects. Biomol Ther. 2022;30:360–7.
44. Viswanathan A, Kute D, Musa A, Konda Mani S, Sipilä V, Emmert-Streib F, et al. 2-(2-(2,4-dioxopentan-3-ylidene)hydrazineyl)benzonitrile as novel inhibitor of receptor tyrosine kinase and PI3K/Akt/mTOR signaling pathway in glioblastoma. Eur J Med Chem. 2019;166:291–303.
45. Nicholson JG, Fine HA. Diffuse glioma heterogeneity and its therapeutic implications. Cancer Discov. 2021;11:575–90.
46. Du ZW. [Establishment of human malignant glioma cell line (SHG-44) and observation on its characteristics]. Zhonghua Zhong Liu Za Zhi Chin J Oncol. 1984;6:241–3.
47. Kojadinovic A, Laderian B, Mundi PS. Targeting TRK: A fast-tracked application of precision oncology and future directions. Crit Rev Oncol/Hematol. 2021;165:103451.